Large-Eddy Simulation of Unsteady Pitching Aerofoil using a One-equation Subgrid Scale (SGS) Model based on Dynamic Procedure

Firdaus Mohamad
Faculty of Mechanical Engineering, Universiti Teknologi MARA (UiTM), 40450 Shah Alam, Selangor, MALAYSIA
firdausmohamad@uitm.edu.my

*Takeo Kajishima**
Department of Mechanical Engineering, Osaka University 2-1 Yamadaoka, Suita, Osaka 565-0871, JAPAN
**kajisima@mech.eng.osaka-u.ac.jp*

ABSTRACT

Large-Eddy Simulations (LES) for an oscillating NACA0012 aerofoil at Reynolds number 1.35 × 10^5 have been performed to investigate the capability of a new approach of a One-equation SGS model. The phenomena of the oscillating aerofoil at higher amplitude angle (α_{amp}) is believed to produce deep dynamic stall in which strong non-equilibrium turbulence could also visible. Hence, a new approach of a one-equation SGS model is proposed where the coefficient of production term in the k_{SGS} transport equation is defined dynamically. From the simulations, the leading-edge vortex (LEV), dynamic stall vortex (DSV), shedding mechanism and trailing edge vortex (TEV) are captured in this study.

Keywords: *LES, Dynamic Stall, One-equation SGS Model, Dynamic Procedure*

Introduction

Predictions of complex flow fields involving both static and dynamic stall are important in a broad range of industrial applications such as turbomachinery, wind turbine aerodynamics, helicopter blade rotors and manoeuvrable wings.

ISSN 1823-5514, eISSN 2550-164X
Received for review: 2020-10-12
Accepted for publication: 2020-11-16
Published: 2021-01-15

Dynamic stall is defined as the phenomenon of exceeding the normal static stall angle. These phenomena are associated with various complex fluid flows such as separations, reattachments and vortex developments which contribute to the unusual aerodynamic characteristics. In terms of turbulence interactions, the dynamic stall produces strong non-equilibrium turbulence in which the turbulence kinetic energy production is imbalanced with the dissipation [1]. Therefore, common subgrid scales (SGS) turbulence models are thought to be insufficient to correctly capture the drastic changes of aerodynamic loads at high angles of attack and moderately high Reynolds numbers.

Experimental works are required to understand and visualize the phenomena of oscillating airfoils. McCroskey et al. [2] conducted an experiment based on oscillating NACA0012 airfoil by using a 7 × 10 ft wind tunnel to investigate the boundary layer separation and vortex shedding mechanism. They concluded that the unsteady separation of the turbulent boundary layer was the primary cause of the vortex shedding mechanism. Lee and Gerontakos [3] executed several experiments to understand the overall flow phenomena of the dynamics stall around an oscillating airfoil. They revealed a clear mechanism of dynamic stall at different stages, such as light-stall oscillating and attached-flow oscillating cases.

Additionally, computational simulations are crucial for any fluid flows analysis. For the dynamic stall simulations, the unsteadiness of boundary layer interaction induced by oscillation can be captured and visualized by means of numerical simulations. Generally, very fine grid density is required to capture all the vortices for the entire dynamic stall process, including unsteady boundary layer separation, transition, shear layer instabilities, laminar separation bubble (LSB) bursting and vortex surface interactions [4], [5]. Thereby, Direct Numerical Simulation (DNS) is a meaningful solution if the computational resources are not a problematical issue. However, as the Re number increases especially for industrial engineering applications such as helicopter blade rotors, wind turbines blades and maneuverable wings [4], [6], the DNS demands tremendous computational capability and memory allocations. Hence the Reynolds-averaged Navier-Stokes (RANS) also can be considered as an option. However, as far as dynamic stall simulation is concerned, the leading-edge transitional flows play an important role in the development of separated flow downstream. Hence, RANS requires an alternative approach to identify the laminar-transition flows by setting the production term to zero prior to available data from experiment. On top of that, the solution of RANS also requires an additional transitional model to predict the transitional flows [4], [7].

Large-eddy simulation (LES) is gaining more attention in studying the complexity of dynamic stall phenomena. A series of comprehensive dynamic stall simulations using LES can be reviewed in Visbal and Garmann [8], Benton and Visbal [9], Visbal and Benton [4] and Visbal [10]. However, none

of these studies were focused on the effect of non-equilibrium of turbulence models. Dindart and Kaynak [11] revealed the importance of a non-equilibrium SGS model to determine the separation and vortex shedding mechanism of the dynamic stall compared to an equilibrium SGS model. A study by Mukai et al. [12] showed that the LES of the Smagorinsky model (SM) with coarse grid spacing in the spanwise direction successfully captured some aspects of the unsteady phenomenon.[12], [13]. Gulillaud et al. [14] also used SM to study the effect of the leading edge vortex (LEV) on the lift coefficient unsteadiness on a pitching NACA0012 at a Reynolds number of 20000. Meanwhile, a Mixed-Time-Scale (MTS) SGS model was used by Almutairi et al. [15] to observe the laminar separation bubbles near the stall of NACA0012 at a Reynolds number of 5×10^4. Their finding shows that an increase of the spanwise domain contributed to intermittent bursting of the laminar separation bubble. Besides, Kim and Xie [16] have also investigated the dynamic stall of NACA0012 using the MTS model to have a better understanding of several factors such as spanwise extension and the effect of freestream turbulence.

To this end, this paper deals with simulations of oscillation airfoils using a new approach of non-equilibrium SGS turbulence model known as a one-equation dynamic (OD) model. NACA0012 airfoil at Reynolds number of 1.35×10^5 was used as a case study to evaluate the turbulence model. Besides, the results of 2 different numbers of grids in a spanwise direction have also been presented.

Governing Equations

In LES, the large-scale flow structures are explicitly solved while the small eddies are numerically modeled. Spatial filtering is commonly used to differentiate between large and small eddies. The spatial filtering or grid filtering is denoted by the overbar ($\bar{f}$) and is described as:

$$\bar{f}(x) = \int_{-\infty}^{\infty} G(y) f(x-y) dy, \tag{1}$$

where the function G is a filter function. The filtered Navier-Stokes equations are defined in non-inertial frame of reference:

$$\frac{\partial \bar{u}_i}{\partial x'_i} = 0, \tag{2}$$

$$\frac{\partial \bar{u}_i}{\partial t} + \frac{\partial (\bar{u}_i + 2\epsilon_{imn}\Omega'_m x'_n)\bar{u}_j}{\partial x'_j} = -\frac{\partial}{\partial x'_i}(\bar{P}) + \nu \frac{\partial^2 \bar{u}_i}{\partial x'_j x'_j} - \frac{\partial \tau_{ij}}{\partial x'_j} - \epsilon_{ijk}\frac{\partial \Omega'_j}{\partial t} x'_k - \epsilon_{ijk}\epsilon_{mnk}\Omega'_j \Omega'_m x'_n \tag{3}$$

where $\bar{P}$ is the effective pressure, ν is the kinematic viscosity, ϵ_{ijk} is Levi-Civita's alternating tensor, $\bar{u}_i$ is the filtered velocity and the Ω'_i is defined as the angular velocity component of the non-inertial system. For the coordinate system, x'_i is derived based on the transformation in non-inertial frame of reference. For this simulation, the axis of rotation is in x_3 direction. The effect of system rotation appears as Coriolis term, centrifugal term and angular acceleration component of the non-inertial system as a result of coordinate transformation for time derivative term and non-linear convective term.

The subgrid-scale (SGS) stress, $\tau_{ij} = \overline{u_i u_j} - \bar{u}_i \bar{u}_j$, appears as a result of filtering in Equation (3) is parameterized by an eddy viscosity model:

$$\tau_{ij} - \frac{\delta_{ij}}{3}\tau_{kk} = -2\upsilon_t \bar{D}_{ij}. \tag{4}$$

Here, δ_{ij} is the Kronecker delta and τ_{kk} is the trace of the SGS stress (added to the pressure term). The υ_t is called the SGS eddy viscosity while the $\bar{D}_{ij}$ is the grid-scale (GS) rate-of-strain tensor:

$$\bar{D}_{ij} = \frac{1}{2}\left(\frac{\partial \bar{u}_i}{\partial x'_j} + \frac{\partial \bar{u}_j}{\partial x'_i}\right). \tag{5}$$

The SGS eddy viscosity is calculated based on:

$$\nu_t = C_\nu \Delta_\nu \sqrt{k_{sgs}} \tag{6}$$

where k_{sgs} is the SGS kinetic energy. The characteristic length in above relation is calculated based on:

$$\Delta_\nu = \frac{\bar{\Delta}}{1 + \frac{C_k \bar{\Delta}^2 \bar{D}^2}{k_{sgs}}} \tag{7}$$

where the grid filter length $\bar{\Delta} = \sqrt[3]{\Delta_1 \Delta_2 \Delta_3}$ is calculated based on the cell volume. The k_{sgs} in Equation (6) is solved by solving the transport equation:

$$\frac{\partial k_{sgs}}{\partial t} + \frac{\partial}{\partial x'_j}\left(\bar{u}_j k_{sgs}\right) = P_{k_{sgs}} - C_\varepsilon \frac{k_{sgs}^{\frac{3}{2}}}{\bar{\Delta}} - \varepsilon_\omega \tag{8}$$

$$+\frac{\partial}{\partial x'_j}\left[\left(\nu + C_d \Delta_v \sqrt{k_{sgs}}\right)\frac{\partial k_{sgs}}{\partial x'_j}\right].$$

This transport equation is also presented in a non-inertial frame of reference. In most studies, the SGS models such as Smagorinsky Model, Dynamic Smagorinsky Model and One-equation SGS kinetic energy are fundamentally based on the assumption that the small scale turbulence is nearly homogeneous and isotropic; hence the rotation effects (Coriolis and Centrifugal) are not counted in the equation [17]. In addition, the impact of system rotation on SGS is less dominant than the local rotation rate of the GS [18], [19]; therefore we made no modification to the model.

In the transport equation of Equation (8), there are 4 terms in the right-hand side that respectively represent the production, the dissipation, the additional dissipation and the diffusion terms. For the production term, $P_{k_{sgs}} = -\tau_{ij}\overline{D}_{ij}$, is responsible for the energy transfer from GS to SGS in the context of the one-equation model. For τ_{ij}, any SGS stress model can be applied. In the case of the eddy viscosity model of Smagorinsky type:

$$P_{k_{sgs}} = 2(c\bar{\Delta}^2|\overline{D}|)\overline{D}_{ij}\overline{D}_{ij} = c\bar{\Delta}^2|\overline{D}|^3. \tag{9}$$

In this study, the dynamic procedure is used to obtain the coefficient, c in Equation (9) in which any smoothing or averaging is not necessary, and thus a negative value of c by Equation (9) is allowed. The negative value indicates the reverse transfer of energy or from SGS to GS portion and it is important for inhomogeneous cases. It is important to note that the negative value of production term will only decrease the k_{SGS}. The backscatter of energy is not represented in the filtered equation of motion because the eddy viscosity ν_t is always positive. For this model, we denoted the model as One-Equation Dynamic Model (OD).

The coefficients for the OD model are $C_\nu = 0.05$, $C_k = 0.08$, $C_\varepsilon = 0.835$ and $C_d = 0.10$. For the detail elaboration for the dynamic procedure such as the test filter that has been used, reader is advice to refer [19], [20].

Computational Setup

This study is focused on dynamic stall simulation around NACA0012 at a Reynolds number of 1.35×10^5 based on chord length and freestream velocity. This range of Reynolds number is believed to still be able to provide a well resolved large-eddy simulation and would be within the range of developed turbulent boundary layer before the dynamic stall takes place [4], [9]. This

setup corresponded to the setup of the wind tunnel experiment conducted by Lee and Gerontakos [3]. Their experiment was conducted based on a 0.15 *m* chord length (*c*) and 2.5*c* span. The freestream velocity was 14 *m/s* and the turbulence intensity of 0.08% was measured at freestream velocity.

In this study, the airfoil performs the pitching motion based on the sinusoidal mode where:

$$\alpha(t) = \alpha_{mean} + \alpha_{amp}\sin\left(\frac{2kU_\infty}{c}t\right). \quad (10)$$

The α_{mean} and α_{amp} represent mean angle of attack and amplitude respectively. The pitching axis is located at quarter chord from the leading edge. The $k = \pi fc/U_\infty$ is reduced frequency. The α_{mean} and α_{amp} were set to 10° and 15° respectively. These prescribed kinematic parameters would result in $\alpha_{min} = -5°$ and $\alpha_{max} = 25°$ where the importance of dynamic stall phenomenon such as LEV, shedding of LEV, trailing-edge vortex (TEV) and the interaction with boundary layer could be evaluated. For the same kinematic parameters, researchers were varied the reduced frequency, *k (0.01-0.4)* [16], [21]–[23], the effect of unsteady freestream velocity [16], grid resolution and domain size effect [16].

Computational Domain and Grid

A typical *C*-type grid is used in this study where ξ coordinate goes around the airfoil and η is in the outward direction from the solid wall and cut-line after the trailing edge. Meanwhile ζ is in the spanwise direction. The domain is extended 0.1*c* in a spanwise direction and had a uniform spacing. A study by Visbal and Garmann [5] showed that the spanwise extension of 0.1*c* was sufficient to capture the LEV and DSV. The domain size for X and Y direction was extended to the 20*c* as shown in Figure 1. This domain extension was found sufficient to hinder the boundary reflections [22].

The grid was designed to have more concentrated nodes near the airfoil to ensure the $y^+ \leq 1$ to capture the boundary layer separation and reattachment. Hence, the height of the first node adjacent to the airfoil wall was set to 1×10^{-4} and 3×10^{-4} around the leading and trailing edge respectively. The finished *C*-mesh around the airfoil, leading and trailing edge is shown in Figure 2. The details of the grid parameter are listed in Table 1.

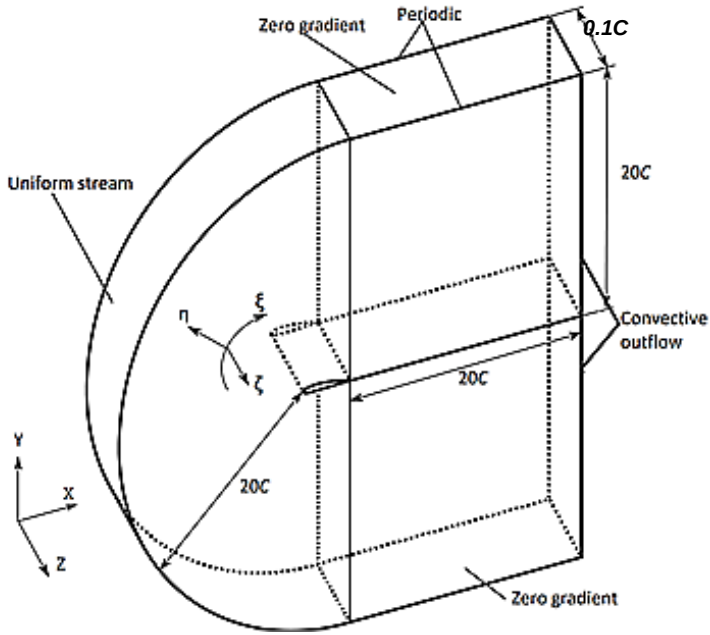

Figure 1: Computational domain and boundary conditions.

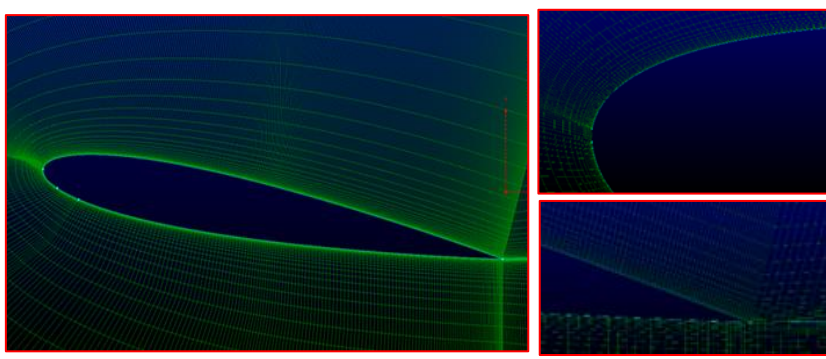

Figure 2: Close up of C-type mesh around NACA0012 (trailing edge and leading edge).

Table 1: Grid Parameters

Grid Type	*C*-grid
# of points along the wake	65
# of points on the pressure side	193
# of points on the suction side	386
# of points on wall normal	50
# of points spanwise	33, 66
L_z/c	0.1

Boundary Conditions

No-slip boundary condition was imposed at the solid wall around the airfoil. The convective outlet boundary condition was used at the velocity outlet. For the inlet, freestream velocity without disturbance was set around the *c*-curve. Periodic boundary condition was applied to the spanwise direction. The computational domain and their respective boundary conditions are shown in Figure 1.

Numerical Procedure

The spatially filtered Navier-Stokes Equations (NSE) were solved using in-house finite difference method code. The influence of rotational effect was added in the momentum equation as shown in Equation (3). The non-linear term was discretized based on Quadratic Upstream Interpolation for Convective Kinematics (QUICK) upwinding scheme. In our calculation, the kinetic energy of SGS transport equation also needed to be solved. For the non-linear term, the donor cell method was adopted. For the diffusion term, 2nd order central finite difference method was applied. In order to solve the temporal discretization, explicit time stepping procedure based on Adams-Bashforth method of the 2nd order accuracy was used. For this calculation, non-dimensional time step was set to $\frac{\Delta t U_\infty}{c} = 3 \times 10^{-5}$ to provide enough temporal resolution of SGS features. The Poisson equation was solved with the SOR (successive over relaxation) method.

Validation Studies

Validation studies have been carried out to confirm the numerical scheme, mesh and solver used in this study. Experimental results by Lee and Gerontakos [3] were used for validation purpose. Pitching motion and Reynolds number were set to $10 + 15\sin(\omega t)$ and $Re = 1.35 \times 10^5$ respectively. Drag coefficient hysteresis is shown in Figure 3. A good satisfactory result between experimental and simulation is observed in the region of attached flows. However, a less satisfactory agreement is further

observed, particularly at higher angle-of-attack. In this region, various flow phenomena are expected such as separation, reattachment and vortex development where the turbulence models used to predict those phenomena play an essential role. This observation is also stressed by Geng et al. [21]. They concluded that the drag coefficient hysteresis results were less satisfactory agreement with experimental results even though a better mesh resolution, turbulence models and time step size were used. Therefore, solver, mesh resolution and the numerical scheme that have been used in this study are within the accepted range.

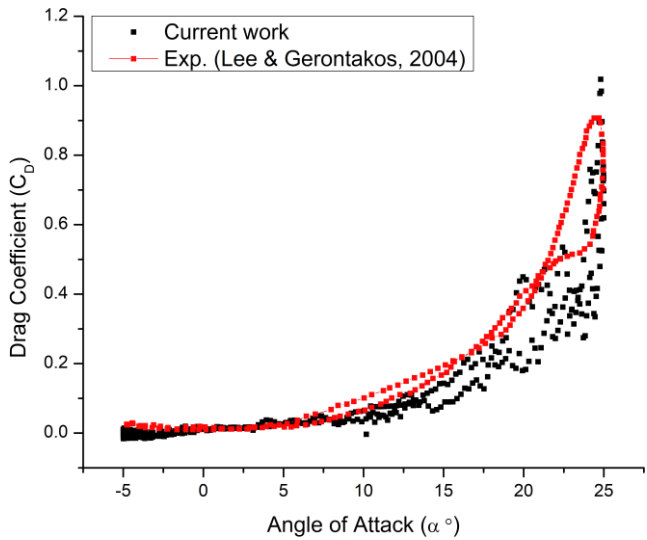

Figure 3: Drag coefficient hysteresis between experimental and simulation.

Results and Discussion

For all computations, the reduced frequency, $k = \pi fc/U_\infty = 0.3$ were set. In order to resolve adequate temporal resolution of fine scale structures, a very small non-dimensional time step was initiated. As a result of these parameters, the non-dimensional period of the motion is $T = 10.5$ where 350000-time steps are required to complete 1 pitching cycle. Due to limitations in computational time, the 3D simulations were running for only 1.5 cycles. This is a common practice for 3D LES simulations for oscillating airfoil where only 1 or 2 cycles were simulated [8], [24].

In order to investigate the effects of grid resolution in the spanwise direction, 2 different grid number were simulated in this study. Figure 4 shows the variation of lift and drag coefficient as a function of non-dimensional flow time (t/T) for N_Z=33 and N_Z=66. Note that symbols '↑' and '↓' refer to upstroke and downstroke motions, respectively. Generally, the drag and lift coefficients are increased during upstroke motion and reaches the peak value at the maximum pitching angle. However, this trend is not identical for drag coefficient where the peak value is observed beyond the maximum angle of attack (around $\alpha = 24° \downarrow$). After reaching the peak value, both drag and lift coefficient exhibit a sudden drop which is representing the dynamic stall. For the simulated operating conditions, a large difference peak value for coefficients between cycle-to-cycle at a high angle of attack during upstroke and downstroke motion is clearly observed. This phenomenon is as expected due to the dynamic stall phenomena such as large separation at trailing edge, effects of transition movement and turbulence [25], [26].

Figure 5 shows time and spanwise averaged pressure coefficients (C_P) for selected upstroke and downstroke pitching motions. The first LEV was detected at 20°↑. The size of the LEV increased as the angle of attack increased. This event led to the vortex shedding mechanism. At the maximum angle of attack 25°↑, the LEV was convected on nearly half of the suction side of the airfoil and at the same time, the DSV also appeared as shown in Figure 5. As a consequence, the airfoil lift dropped.

In the region of the downstroke phase, the vortex was shedding downstream. At 17°↓, the counter rotating vortex appeared at the trailing edge. This counter-rotating vortex also increased in size as the angle of attack decreased. This could be seen in pressure distribution where the suction pressure peaked at the trailing edge. Finally, this vortex merged with the first LEV and convected into the wake. At this angle of attack, the lift and drag continued to decrease.

The Q-criterion [27] is used to observe vortical phenomena in dynamic stall simulations. The unsteady flowfield for the upstroke and downstroke phases based on Q-criterion coloured by streamwise velocity are shown in Figure 6. Beginning from 15°↑, development of transitional flow field was observed (marked as 'a'). At 18°↑, a fine scale structure resulting from spanwise coherent structures from the transition region was formed. This observation was also discussed in detail in the work of [10]. The formation of the LEV was as shown at 21°↑. At the maximum angle of attack (25.0°↑), the LEV became larger and convected downstream. At this angle, the airfoil no longer produced lift. Besides, the formation of DSV also could be seen for the downstroke phase.

Overall, phenomena which occurred around the pitching airfoil was observed vto be similar to the N_z=33. Figure 7 shows the iso-surfaces of Q-criterion based on streamwise velocity for some selected angles of the pitching

motion. The hairpin-like vortices were captured during both upstroke and downstroke motions. As a result of vortices breaking down, finer and random well-developed turbulent structures [28] were observed downstream of the airfoil suction side. Additionally, Kobayashi et al. [29] elaborated that hairpin vortices were related to the forward and backwards scatter events. Hence, the non-equilibrium of the SGS model introduced in the OD model was useful in capturing these vortices. For pressure distribution curves, no apparent differences were observed for both grids (not shown here).

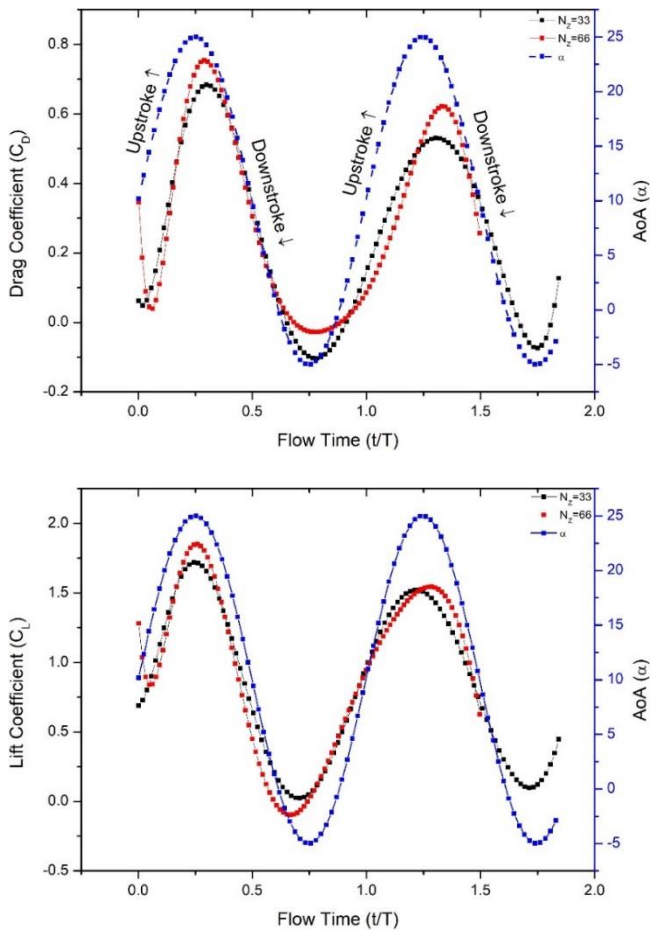

Figure 4: Coefficient of drag (C_D) and lift (C_L) versus non-dimensional flow time (t/T). The Angle-of-attack (AoA) is on the right axis.

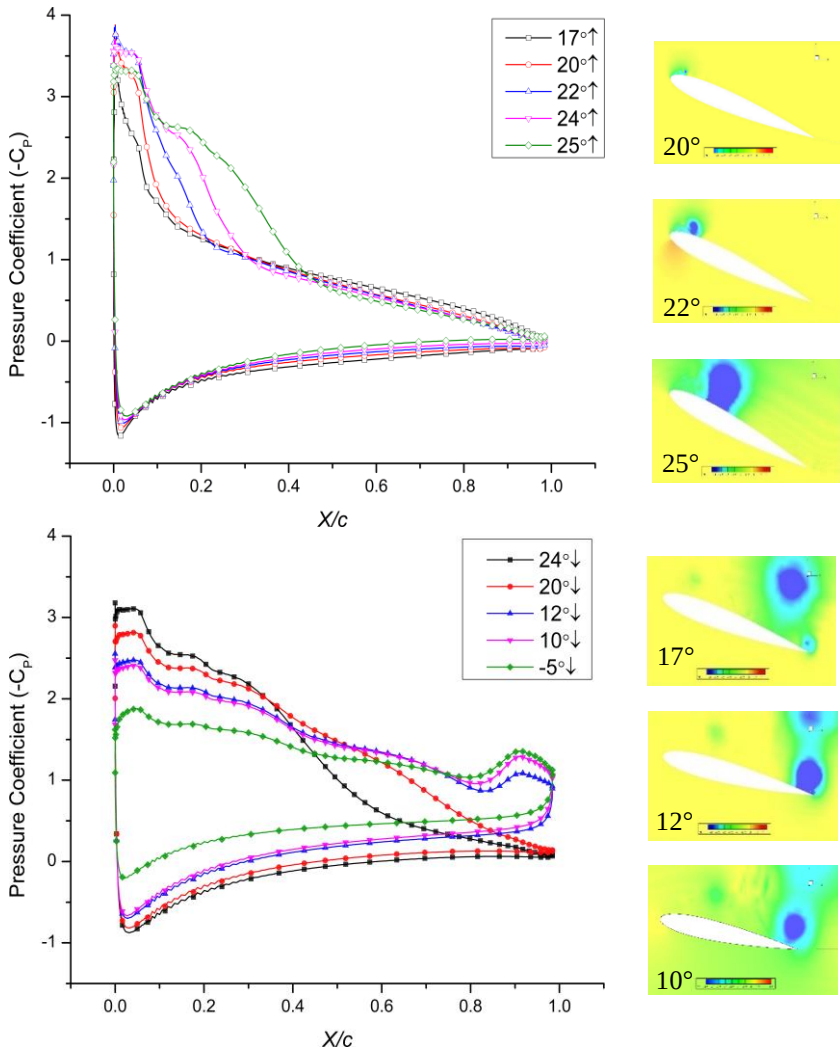

Figure 5: Time and Spanwise-Averaged Pressure Coefficient (C_P) for selected upstroke and downstroke angles (Grid N_z=33).

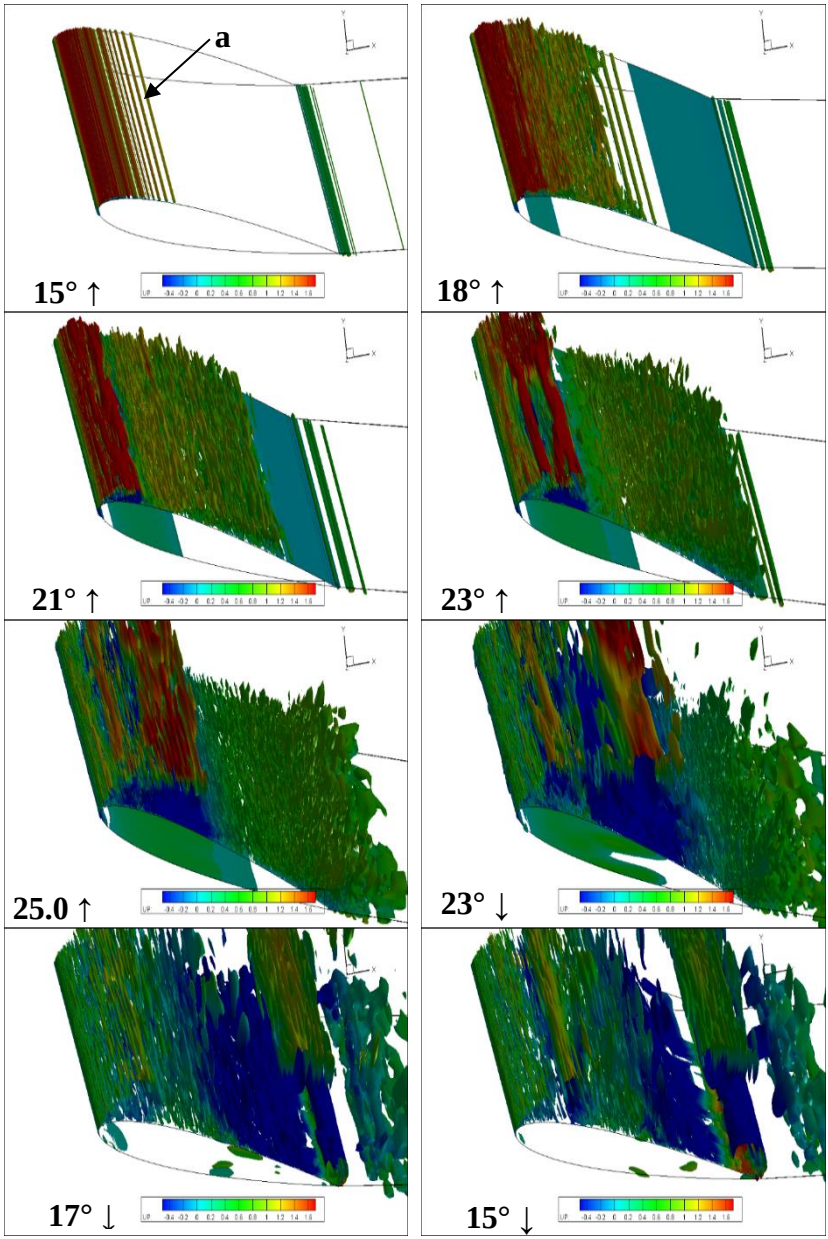

Figure 6: Iso-surfaces of Q-criterion colored by streamwise velocity for selected angles (Grid N_z=33).

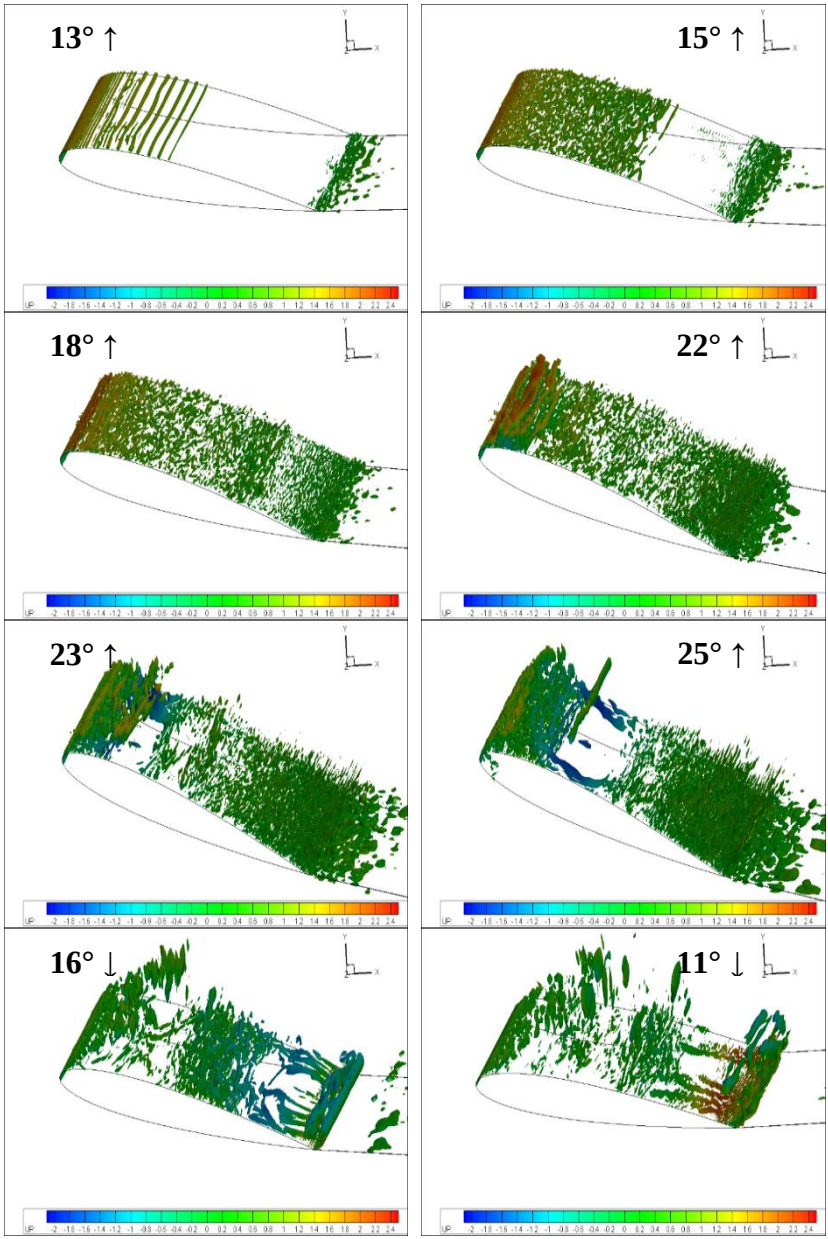

Figure 7: Iso-surfaces of Q-criterion colored by streamwise velocity for selected angles (Grid N_z=66).

Conclusion

LES over an oscillating NACA0012 airfoil were performed to evaluate the performance of a dynamic approach of a one-equation SGS model. Two different grids were used in this study to evaluate the resolution effects in the spanwise direction. It is observed that no significant differences can be seen in forces and pressure coefficients. However, increasing the number of spanwise direction to 66 led to an exciting finding where the hairpin vortices were captured for both upstroke and downstroke motions. On top of that, introducing the dynamic procedure in non-equilibrium SGS model is found useful in the leading edge transitional region. The laminar separation bubble, separation and reattachment were captured during the unsteady motion and can be seen in the pressure coefficient plots. The finding in this study could be more elaborated in terms of hysteresis forces if more cycles can be simulated. However, due to the limitations in computational capacity, only 1.5 cycles were simulated. Despite this, the findings of the present study could be served as a guideline to evaluate the effects of non-equilibrium SGS model with a variation of reduced frequency and grid resolution subjected to the moderate Reynolds number and deep dynamic stall problems.

Acknowledgements

The first author would like to acknowledge the Malaysia Government through Ministry of Higher Education (MoHE) and Universiti Teknologi MARA (UiTM) for financial support through its scholarship program (SLAB). The author is also grateful to Yasuaki Kaneko and Takeshi Omori for sharing their valuable knowledge and information about the simulations.

References

[1] G. Martinat, M. Braza, Y. Hoarau, and G. Harran, "Turbulence Modelling of the Flow Past a Pitching NACA0012 Airfoil at 10^5 and 10^6 Reynolds Numbers," *J. Fluids Struct.*, vol. 24, no. 8, pp 1294–1303, 2008.

[2] W. J. McCroskey, L. W. Carr, and K. W. McAlister, "Dynamic Stall Experiments on Oscillating Airfoils," *AIAA J.*, vol. 14, no. 1, pp 57–63, 2008.

[3] T. Lee and P. Gerontakos, "Investigation of Flow Over an Oscillating Airfoil," *J. Fluid Mech.*, vol. 512, pp 313–341, 2004.

[4] M. R. Visbal and S. I. Benton, "Exploration of High-Frequency Control of Dynamic Stall Using Large-Eddy Simulations," *AIAA J.*, vol. 56, no. 8, pp 2974–2991, 2018.

[5] M. R. Visbal and D. J. Garmann, "Analysis of Dynamic Stall on a Pitching Airfoil Using High-Fidelity Large-Eddy Simulations," *AIAA J.*, vol. 56,

no. 1, pp 46–63, 2017.
[6] K. Gharali and D. A. Johnson, "Dynamic Stall Simulation of a Pitching Airfoil under Unsteady Freestream Velocity," *J. Fluids Struct.*, vol. 42, pp 228–244, Oct. 2013.
[7] J. A. Ekaterinaris and F. R. Menter, "Computation of Oscillating Airfoil Flows with One- and Two-Equation Turbulence Models," *AIAA J.*, vol. 32, no. 12, pp 2359–2365, Dec. 1994.
[8] M. R. Visbal and D. J. Garmann, "Investigation of Spanwise End Effects on Dynamic Stall of a Pitching Wing Section," *J. Aircr.*, pp 1–13, 2019.
[9] S. I. Benton and M. R. Visbal, "Extending the Reynolds Number Range of High-frequency Control of Dynamic Stall," *AIAA J.*, vol. 57, no. 7, pp 2675–2681, 2019.
[10] M. R. Visbal, "Analysis of the Onset of Dynamic Stall using High-fidelity Large-Eddy Simulations," *52nd Aerosp. Sci. Meet.*, no. January, pp 1–25, 2014.
[11] M. Dindart and U. Kaynak, "Effect of Turbulence Modeling on Dynamic Stall of a NACA0012 Airfoil," in *30th Aerospace Sciences Meeting & Exhibit*, pp 1–14.
[12] J. Mukai, S. Enomoto, and T. Aoyama, "Large-Eddy Simulation of Natural Low-frequency Flow Oscillations on an Airfoil near Stall," *Collect. Tech. Pap. - 44th AIAA Aerosp. Sci. Meet.*, vol. 22, no. January, pp 17066–17075, 2006.
[13] J. H. Almutairi and I. M. AlQadi, "Large-Eddy Simulation of Natural Low-Frequency Oscillations of Separating–Reattaching Flow Near Stall Conditions," *AIAA J.*, vol. 51, no. 4, pp. 981–991, Apr. 2013.
[14] N. Guillaud, G. Balarac, and E. Goncalvès, "LES on a Pitching Airfoil: Analysis of the Lift Coefficient Unsteadiness," *Notes Numer. Fluid Mech. Multidiscip. Des.*, vol. 135, pp. 163–169, 2018.
[15] J. H. Almutairi, L. E. Jones, and N. D. Sandham, "Intermittent bursting of a laminar separation bubble on an airfoil," *AIAA J.*, vol. 48, no. 2, pp. 414–426, 2010.
[16] Y. Kim and Z. T. Xie, "Modelling the effect of freestream turbulence on dynamic stall of wind turbine blades," *Comput. Fluids*, vol. 129, pp. 53–66, 2016.
[17] H. Lu, C. J. Rutland, and L. M. Smith, "A posteriori tests of one-equation les modeling of rotating turbulence," *Int. J. Mod. Phys. C*, vol. 19, no. 12, pp. 1949–1964, 2008.
[18] M. Tsubokura, T. Kobayashi, N. Taniguchi, and T. Kogaki, "Subgrid scale modeling for turbulence in rotating reference frames," *J. Wind Eng. Ind. Aerodyn.*, vol. 81, no. 1–3, pp. 361–375, 1999.
[19] T. Kajishima and T. Nomachi, "One-Equation Subgrid Scale Model using Dynamic Procedure for the Energy Production," *J. Appl. Mech.*, vol. 73, no. 3, pp. 368–373, 2006.

[20] F. Mohamad and T. Kajishima, "Large eddy simulation using one-equation SGS model based on dynamic procedure for flows in laminar-transition region," *J. Adv. Res. Fluid Mech. Therm. Sci.*, vol. 60, no. 2, pp. 166–177, 2019.

[21] F. Geng, I. Kalkman, A. S. J. Suiker, and B. Blocken, "Sensitivity Analysis of Airfoil Aerodynamics during Pitching Motion at a Reynolds Number of 1.35×10 5," *J. Wind Eng. Ind. Aerodyn.*, vol. 183, pp. 315–332, Dec. 2018.

[22] S. Wang, D. B. Ingham, L. Ma, M. Pourkashanian, and Z. Tao, "Turbulence Modeling of Deep Dynamic Stall at relatively Low Reynolds Number," *J. Fluids Struct.*, vol. 33, pp. 191–209, 2012.

[23] X. Li, D. Grecov, Z. Guo, and Z. Hou, "Influence of Unsteady and Kinematic Parameters on Aerodynamic Characteristics of a Pitching Airfoil," *J. Aerosp. Eng.*, vol. 32, no. 1, pp 1–11, 2019.

[24] M. Sánchez-Rocha, M. Kirtaş, and S. Menon, "Zonal hybrid RANS-LES Method for Static and Oscillating Airfoils and Wings," *Collect. Tech. Pap. - 44th AIAA Aerosp. Sci. Meet.*, vol. 20, no. January, pp 15211–15231, 2006.

[25] Y. Shida, K. Kuhawahara, K. Ono, and H. Takami, "Computation of Dynamic Stall of a NACA-0012 Airfoil," *AIAA J.*, vol. 25, no. 3, pp 408–413, 1987.

[26] H. Liang, X. Wang, L. Zou, and Z. Zong, "Numerical study of two-dimensional heaving airfoils in ground effect," *J. Fluids Struct.*, vol. 48, pp 188–202, 2014.

[27] J. JEong and F. Hussain, "On the Identification of a Vortex," *J. Fluid Mech.*, vol. 285, no. February, pp 69–94, 1995.

[28] S. Kawai and K. Asada, "Wall-modeled Large-Eddy Simulation of High Reynolds Number Flow around an Airfoil near Stall Condition," *Comput. Fluids*, vol. 85, pp 105–113, 2013.

[29] H. Kobayashi, F. Ham, and X. Wu, "Application of a Local SGS Model based on Coherent Structures to Complex Geometries," *Int. J. Heat Fluid Flow*, vol. 29, no. 3, pp 640–653, 2008.